

# Outage Probability Analysis of Uplink NOMA over Ultra-High-Speed FSO-Backhauled Systems

Mohammad Vahid Jamali<sup>1</sup>, Seyed Mohammad Azimi-Abarghouyi<sup>2</sup>, and Hessam Mahdavi<sup>1</sup>

<sup>1</sup>EECS Department, University of Michigan, Ann Arbor, MI 48109, USA (mvjamali@umich.edu, hessam@umich.edu)

<sup>2</sup>Sharif University of Technology, Tehran, Iran (e-mail: azimi\_sm@ee.sharif.edu)

**Abstract**—In this paper, we consider a relay-assisted uplink non-orthogonal multiple access (NOMA) system where two radio frequency (RF) users are grouped for simultaneous transmission, over each resource block, to an intermediate relay which forwards the amplified version of the users' aggregated signals in the presence of multiuser interference to a relatively far destination. In order to cope with the users' ever-increasing desire for higher data rates, a high-throughput free-space optics (FSO) link is employed as the relay-destination backhaul link. Dynamic-order decoding is employed at the destination to determine the priority of the users based on their instantaneous channel state information (CSI). Closed-form expressions for the individual- and sum-rate outage probability formulas are derived in the case of independent Rayleigh fading for the users-relay access links when the FSO backhaul link is subject to Gamma-Gamma turbulence with pointing error. This work can be regarded as an initial attempt to incorporate power-domain NOMA over ultra-high-speed FSO-backhauled systems, known as mixed RF-FSO systems.

## I. INTRODUCTION

Non-orthogonal multiple access (NOMA) is being considered as one of the enabling technologies for the fifth generation (5G) wireless networks. With its two general power- and code-domain forms, NOMA can potentially pave the way toward higher throughput, lower latency, improved fairness, higher reliability, and massive connectivity [1]. Motivated by these fascinating advantages, extensive research activities have been carried out in the past few years to promote the NOMA advancement in diverse directions (see, e.g., [2] for a comprehensive survey).

In a variety of applications, there is a need to transmit the users' data to a central unit (CU) or a wired base station (BS) while, given the limited power of the users, it is not feasible for the users to directly communicate with the relatively far destination. Motivated by this fact, several recent work have dealt with the relaying problem in downlink and uplink NOMA communications. In particular, capacity analysis of a simple cooperative relaying system, consisting of a source, a relay, and a destination is provided in [3]. The outage probabilities and ergodic sum rate of a downlink two-user NOMA system, with a full-duplex relay helping one of the users, is characterized in [4]. Performance of downlink NOMA transmission with an intermediate amplify-and-forward (AF) relay for multiple-antenna systems, and over Nakagami- $m$  fading channels is investigated in [5] and [6], respectively. The performance of coordinated direct and relay transmission for two-user downlink and uplink NOMA systems is investigated in [7] and [8], respectively. Hybrid decode-and-forward (DF) and AF relaying in NOMA systems is proposed in [9], and forwarding strategy selection is explored in [10]. Additionally, in order to enable NOMA technology for massive communications, primary

work on power-domain NOMA can be mixed with the low-complexity recursive approach proposed in [11] based on the Kronecker product of NOMA pattern matrices.

All of the aforementioned work consider sub-6 GHz radio frequency (RF) band for the backhaul link through an AF or DF relay in the absence of any external multiuser interference to the NOMA users. However, the scarce available bandwidth in the sub-6 GHz band will not be able to support the users' aggressive demand for the higher data rates, especially when NOMA is employed in the users-relay access links to provide higher throughput for the users. In this case, the relay-destination backhaul link can pose a severe bottleneck on the end-to-end performance and substantially negate the NOMA advantages through reducing the users' achievable throughput and reliability which can in turn even increase their latency.

A potential approach to overcome the aforementioned drawback is moving to higher frequency bands, e.g., through the deployment of millimeter-wave [12] or free-space optics (FSO) backhaul links [13]. Millimeter-wave communication is usually preferred for relatively shorter communication lengths due to the severe propagation conditions at millimeter frequencies [14]. FSO links, on the other hand, can provide much more available bandwidth and support ranges on the order of several kilometers [15].

In this paper, we investigate the outage probability performance of uplink NOMA transmission over mixed RF-FSO systems when an AF relay is employed to forward the amplified received signal from the Rayleigh fading access links to the destination through an ultra-high-throughput directive interference-free FSO link subject to Gamma-Gamma (GG) fading with beam misalignment error. We consider a two-user uplink NOMA system where the communication is subject to the presence of multiuser interference from some independent users. Such interference can be induced, e.g., due the co-channel interference from some nearby users aiming to communicate with some other relays or destinations. We apply dynamic-order decoding, also employed very recently in [16], [17], to dynamically determine the detection order of the NOMA users at the destination, and then derive the closed-form expressions for the individual- and sum-rate outage probabilities. This paper can be considered as an initial attempt to incorporate power-domain NOMA in mixed RF-FSO systems.

The rest of the paper is organized as follows. In Section II, we describe the system model. In Section III, we derive the individual- and sum-rate outage probability closed-form formulas for uplink NOMA over mixed-RF-FSO system. Section IV provides the numerical results, and Section V concludes the paper.

## II. SYSTEM MODEL

Consider two RF users  $\mathcal{U}_1$  and  $\mathcal{U}_2$  grouped together for uplink NOMA transmission to an AF relay  $\mathcal{R}$ . Denote the composite channel gain of the  $\mathcal{U}_i - \mathcal{R}$  link by  $h_i = \sqrt{L_i} \tilde{h}_i$ ,  $i = 1, 2$ , where  $L_i$  and  $\tilde{h}_i$  are respectively the path loss gain and independent-and-identically-distributed (iid) Rayleigh fading coefficient of the  $\mathcal{U}_i - \mathcal{R}$  RF link given by [18, Eq. (2)]. Furthermore, assume that the uplink transmission to the relay is affected by undesired multiuser interference from  $K$  interfering users  $\mathcal{I}_k$ ,  $k = 1, 2, \dots, K$ , each with the transmit power  $p'_k$ , path loss gain  $L'_k$ , and iid Rayleigh fading coefficient  $\tilde{h}'_k$ . This interference can be from the users scheduled for the concurrent transmission to some other relays in the cellular network or any other non-vanishing interference during the desired transmission block. The received signal by the relay is then expressed as

$$y_{\mathcal{R}} = \sum_{i=1}^2 x_i \tilde{h}_i \sqrt{a_i L_i P} + \sum_{k=1}^K x'_k \tilde{h}'_k \sqrt{L'_k p'_k} + n_{\mathcal{R}}, \quad (1)$$

where  $x_i$  and  $x'_k$  are the transmit symbols by  $\mathcal{U}_i$  and  $\mathcal{I}_k$ , respectively, and  $n_{\mathcal{R}}$  is the additive white Gaussian noise (AWGN) of the relay receiver with mean zero and variance  $\sigma_{\mathcal{R}}^2$ . Moreover,  $a_1$  and  $a_2 = 1 - a_1$  are the power allocation coefficients determining the portion of the total power  $P$  assigned to each of the desired users. Note that for the users with independent Rayleigh fading, all fading gains  $|\tilde{h}_i|^2$ 's and  $|\tilde{h}'_k|^2$ 's have an exponential distribution with mean one (to ensure that fading neither amplifies nor attenuates the received power) as  $f_{|\tilde{h}_i|^2}(x) = f_{|\tilde{h}'_k|^2}(x) = \exp(-x)$ ,  $x \geq 0$ . Note that, in this paper, for the sake of simplicity, we do not consider the stochastic geographical positions of the nodes, and deal with the building part of the analysis, corresponding to a given time slot, where the nodes are at some fixed positions.

The received signal  $y_{\mathcal{R}}$  at the relay is then converted to optical signal using intensity-modulation direct-detection (IM/DD), and is amplified with a constant gain  $G$  to keep the disparity between the power level of different NOMA users for successive interference cancellation (SIC) detection at the destination. In this case, the transmitted optical signal by the relay toward the destination  $\mathcal{D}$  can be expressed as  $S_{\mathcal{R}} = G(1 + \eta y_{\mathcal{R}})$ , where  $\eta$  is the electrical-to-optical conversion coefficient [19]. The transmitted signal then undergoes the composite FSO channel gain of  $g = g_l \tilde{g}$  where  $g_l$  is the path loss gain of the  $\mathcal{R} - \mathcal{D}$  FSO backhaul link, with length  $d_{\mathcal{R}\mathcal{D}}$ , defined as  $g_l = \rho \times 10^{-\kappa d_{\mathcal{R}\mathcal{D}}/10}$  where  $\rho$  is the responsivity of the photodetector, and  $\kappa$  is the weather-dependent attenuation coefficient [18]. Moreover,  $\tilde{g} = g_p g_f$  is the total fading coefficient due to pointing error  $g_p$  and optical turbulence  $g_f$ . In the case of GG optical turbulence with beam misalignment, the distribution of  $\tilde{g}$  can be expressed as [20]

$$f_{\tilde{g}}(\tilde{g}) = \frac{\alpha \beta \xi^2}{A_0 \Gamma(\alpha) \Gamma(\beta)} G_{1,3}^{\alpha, \beta} \left[ \frac{\alpha \beta}{A_0} \tilde{g} \middle| \xi^2 - 1, \alpha - 1, \beta - 1 \right], \quad (2)$$

where  $\alpha$  and  $\beta$  are the fading parameters of the GG distribution,  $\xi$  is the ratio of the equivalent beam radius and the pointing error displacement standard deviation (jitter) measured at the receiver,  $\Gamma(\cdot)$  is the Gamma function [21, Eq. (8.310)], and  $G[\cdot]$  is the Meijer's G-function [21, Eq. (9.301)]. Furthermore,  $A_0$  is the geometric loss in the case of perfect beam alignment (zero radial displacement) defined as  $A_0 = [\text{erf}(\sqrt{\pi r}/(\sqrt{2} \phi d_{\mathcal{R}\mathcal{D}}))]^2$

in which  $\text{erf}(\cdot)$  is the error function,  $r$  is the receiver aperture radius, and  $\phi$  is the transmitter beam divergence angle. The destination then filters out the direct current (DC) component of  $g_l \tilde{g} G$  from  $g_l \tilde{g} S_{\mathcal{R}} + n_{\mathcal{D}}$  to obtain the received signal as

$$y_{\mathcal{D}} = \eta g_l \tilde{g} G \left( \sum_{i=1}^2 x_i \tilde{h}_i \sqrt{a_i L_i P} + \sum_{k=1}^K x'_k \tilde{h}'_k \sqrt{L'_k p'_k} + n_{\mathcal{R}} \right) + n_{\mathcal{D}}, \quad (3)$$

where  $n_{\mathcal{D}}$  is the destination AWGN with mean zero and variance  $\sigma_{\mathcal{D}}^2$ .

We assume that the NOMA users are indexed based on their path loss gains, i.e.,  $L_1 \geq L_2$ , and the power allocation strategy proposed in [22] is adopted to determine  $a_1$  and  $a_2$  as  $a_1 L_1 = a_2 L_2 \times 10^{s/10}$  where  $s \geq 0$  is the power back-off step; hence,  $a_1 = L_2 \times 10^{s/10} / (L_1 + L_2 \times 10^{s/10})$ , and  $a_2 = L_1 / (L_1 + L_2 \times 10^{s/10})$ . We further assume that the BS has perfect knowledge about the channel state information (CSI) and orders the NOMA users based on their instantaneous received power. In fact, based on the principles of uplink power-domain NOMA [22], [23], the BS orders the users based on their channel conditions from best to worst. Such a dynamically ordering the users can potentially prevent the possibility of firstly decoding the users with worse instantaneous channel conditions if they are fixedly ordered based on their channel statistics. Therefore, depending on the fading coefficients  $\tilde{h}_1$  and  $\tilde{h}_2$ , the detection order is either  $\pi_1 = (1, 2)$ , meaning that the first user is decoded first, if  $a_1 L_1 |\tilde{h}_1|^2 \geq a_2 L_2 |\tilde{h}_2|^2$  or  $\pi_2 = (2, 1)$  if otherwise.

## III. OUTAGE PROBABILITY ANALYSIS

In this section, we characterize the individual- and sum-rate outage probability formulas for dual-hop uplink NOMA over mixed RF-FSO systems.

### A. Individual-Rate Outage Analysis

Note that if the detection order is  $\pi_1$ , the SIC receiver first treats the signal from the second NOMA user as noise to decode  $x_1$  with the signal-to-interference-plus-noise ratio (SINR) of

$$\gamma_{\pi_1}^{(1)} = \frac{a_1 L_1 P \tilde{g}^2 |\tilde{h}_1|^2}{a_2 L_2 P \tilde{g}^2 |\tilde{h}_2|^2 + \sum_{k=1}^K L'_k p'_k \tilde{g}^2 |\tilde{h}'_k|^2 + \tilde{g}^2 \sigma_{\mathcal{R}}^2 + C_{\mathcal{D}}}, \quad (4)$$

and then, after removing the received power from the first user, decodes  $x_2$  with the SINR of

$$\gamma_{\pi_1}^{(2)} = \frac{a_2 L_2 P \tilde{g}^2 |\tilde{h}_2|^2}{\sum_{k=1}^K L'_k p'_k \tilde{g}^2 |\tilde{h}'_k|^2 + \tilde{g}^2 \sigma_{\mathcal{R}}^2 + C_{\mathcal{D}}}, \quad (5)$$

where  $C_{\mathcal{D}} = \sigma_{\mathcal{D}}^2 / (\eta^2 g_l^2 G^2)$ . Similarly, when the detection order is  $\pi_2$  the SINR values  $\gamma_{\pi_2}^{(1)}$  and  $\gamma_{\pi_2}^{(2)}$  can be obtained by appropriate change of indexes in (4) and (5).

The outage probability of the first user  $\mathcal{U}_1$  in achieving an individual rate of  $R_{\text{th}}^{(1)}$  can be characterized as

$$\begin{aligned} P_{\text{out}}^{(1)} &\stackrel{(a)}{=} P(\pi_1) P_{\text{out}|\pi_1}^{(1)} + P(\pi_2) P_{\text{out}|\pi_2}^{(1)} \\ &\stackrel{(b)}{=} 1 - \left[ \Pr(\gamma_{\pi_1}^{(1)} > \gamma_{\text{th}}^{(1)}, \pi_1) + \right. \\ &\quad \left. \Pr(\gamma_{\pi_2}^{(2)} > \gamma_{\text{th}}^{(2)}, \pi_2) \times \Pr(\gamma_{\pi_2}^{(1)} > \gamma_{\text{th}}^{(1)}, \pi_2) / P(\pi_2) \right], \quad (6) \end{aligned}$$

where step (a) follows from the law of total probability by defining  $P_{\text{out}|\pi_i}^{(1)}$ ,  $i = 1, 2$ , as the conditional outage probability

$$\begin{aligned}
& \Pr(\gamma_{\pi_1}^{(1)} < \gamma_{\text{th}}^{(1)}, \pi_1) \Big|_{\gamma_{\text{th}}^{(1)} < 1} \stackrel{(a)}{=} \Pr\left(|\tilde{h}_1|^2 < \gamma_{\text{th}}^{(1)} \left[|\tilde{h}_2|^2 \times 10^{-s/10} + \mathcal{I}_1 + C_{\mathcal{D}}/(a_1 L_1 P \tilde{g}^2)\right], |\tilde{h}_1|^2 \geq |\tilde{h}_2|^2 \times 10^{-s/10}\right) \\
& \stackrel{(b)}{=} \mathbb{E}_{|\tilde{h}_2|^2 < J_{\text{th}}^{(1)}(\mathcal{I}_1 + C_{\mathcal{D}}/(a_1 L_1 P \tilde{g}^2))} \left[ \exp\left(-|\tilde{h}_2|^2 \times 10^{-s/10}\right) - \exp\left(-\gamma_{\text{th}}^{(1)} \left[|\tilde{h}_2|^2 \times 10^{-s/10} + \mathcal{I}_1 + C_{\mathcal{D}}/(a_1 L_1 P \tilde{g}^2)\right]\right) \right] \\
& = \mathbb{E}_{\mathcal{I}_1, \tilde{g}} \left[ \left(1 + 10^{-s/10}\right)^{-1} \times \left[1 - \exp\left(-\left[1 + 10^{-s/10}\right] J_{\text{th}}^{(1)}(\mathcal{I}_1 + C_{\mathcal{D}}/(a_1 L_1 P \tilde{g}^2))\right)\right] \right] \\
& - \mathbb{E}_{\mathcal{I}_1, \tilde{g}} \left[ \left(1 + \gamma_{\text{th}}^{(1)} \times 10^{-s/10}\right)^{-1} \times \left[1 - \exp\left(-\left[1 + \gamma_{\text{th}}^{(1)} \times 10^{-s/10}\right] J_{\text{th}}^{(1)}(\mathcal{I}_1 + C_{\mathcal{D}}/(a_1 L_1 P \tilde{g}^2))\right)\right] \exp\left(-\gamma_{\text{th}}^{(1)} \left[\mathcal{I}_1 + C_{\mathcal{D}}/(a_1 L_1 P \tilde{g}^2)\right]\right) \right] \\
& \stackrel{(c)}{=} \frac{10^{s/10}}{1 + 10^{s/10}} \left(1 - \exp\left(\frac{-J_{\text{th},1}^{(1)} \sigma_{\mathcal{R}}^2}{a_1 L_1 P}\right)\right) \mathbb{E}_{\tilde{g}} \left[ \exp\left(\frac{-J_{\text{th},1}^{(1)} C_{\mathcal{D}}}{a_1 L_1 P \tilde{g}^2}\right) \right] \prod_{k=1}^K \frac{a_1 L_1 P}{a_1 L_1 P + J_{\text{th},1}^{(1)} L'_k p'_k} - \frac{10^{s/10}}{\gamma_{\text{th}}^{(1)} + 10^{s/10}} \left(\exp\left(\frac{-\gamma_{\text{th}}^{(1)} \sigma_{\mathcal{R}}^2}{a_1 L_1 P}\right)\right) \\
& \times \mathbb{E}_{\tilde{g}} \left[ \exp\left(\frac{-\gamma_{\text{th}}^{(1)} C_{\mathcal{D}}}{a_1 L_1 P \tilde{g}^2}\right) \right] \prod_{k=1}^K \frac{a_1 L_1 P}{a_1 L_1 P + \gamma_{\text{th}}^{(1)} L'_k p'_k} - \exp\left(\frac{-\sigma_{\mathcal{R}}^2 J_{\text{th},2}^{(1)}}{a_1 L_1 P}\right) \mathbb{E}_{\tilde{g}} \left[ \exp\left(\frac{-C_{\mathcal{D}} J_{\text{th},2}^{(1)}}{a_1 L_1 P \tilde{g}^2}\right) \right] \prod_{k=1}^K \frac{a_1 L_1 P}{a_1 L_1 P + L'_k p'_k J_{\text{th},2}^{(1)}}. \quad (7)
\end{aligned}$$

of the first NOMA user given the decoding order  $\pi_i$ . Moreover, in step (a),  $P(\pi_1) = \Pr(|\tilde{h}_1|^2 \geq |\tilde{h}_2|^2 \times 10^{-s/10}) = \mathbb{E}_{|\tilde{h}_2|^2} [\exp(-|\tilde{h}_2|^2 \times 10^{-s/10})] = (1 + 10^{-s/10})^{-1}$ , and  $P(\pi_2) = 1 - P(\pi_1) = (1 + 10^{s/10})^{-1}$  are the probabilities of having decoding orders  $\pi_1$ , and  $\pi_2$ , respectively. Furthermore, step (b) follows, first, by defining  $P_{\text{cov}|\pi_i}^{(1)} = 1 - P_{\text{out}|\pi_i}^{(1)}$ ,  $i = 1, 2$ , as the probability of successfully achieving  $R_{\text{th}}^{(1)}$  for  $\mathcal{U}_1$  conditioned on the decoding order  $\pi_i$ , and then noting that correct detection of  $x_1$  for the decoding order  $\pi_2 = (2, 1)$  requires successful decoding of the preceding symbol  $x_2$ , i.e.,  $P_{\text{cov}|\pi_1}^{(1)} = \Pr(\gamma_{\pi_1}^{(1)} > \gamma_{\text{th}}^{(1)} | \pi_1)$  and  $P_{\text{cov}|\pi_2}^{(1)} = \Pr(\gamma_{\pi_2}^{(2)} > \gamma_{\text{th}}^{(2)} | \pi_2) \times \Pr(\gamma_{\pi_2}^{(1)} > \gamma_{\text{th}}^{(1)} | \pi_2)$  where  $\gamma_{\text{th}}^{(i)}$  is the threshold SINR for an IM/DD FSO link to achieve the desired data rate  $R_{\text{th}}^{(i)}$ ,  $i = 1, 2$ . In the following, we calculate the three joint probabilities in (6) to ascertain the outage probability of the first user  $\mathcal{U}_1$ .

In order to calculate  $\Pr(\gamma_{\pi_1}^{(1)} > \gamma_{\text{th}}^{(1)}, \pi_1)$  we first note that  $\Pr(\gamma_{\pi_1}^{(1)} > \gamma_{\text{th}}^{(1)}, \pi_1) = P(\pi_1) \Pr(\gamma_{\pi_1}^{(1)} > \gamma_{\text{th}}^{(1)} | \pi_1) = P(\pi_1) [1 - \Pr(\gamma_{\pi_1}^{(1)} < \gamma_{\text{th}}^{(1)} | \pi_1)] = P(\pi_1) - \Pr(\gamma_{\pi_1}^{(1)} < \gamma_{\text{th}}^{(1)}, \pi_1)$ . Then using (4),  $\Pr(\gamma_{\pi_1}^{(1)} < \gamma_{\text{th}}^{(1)}, \pi_1)$  can be calculated as (7) shown at the top of this page where, in step (a),  $\mathcal{I}_1 = (\sum_{k=1}^K L'_k p'_k |\tilde{h}'_k|^2 + \sigma_{\mathcal{R}}^2)/(a_1 L_1 P)$  is the sum of the power of multiuser interference and noise, at the relay, normalized to the average power of the first NOMA user. Moreover, step (b) follows, first, by defining the constant  $J_{\text{th}}^{(1)} = 10^{s/10} \times \gamma_{\text{th}}^{(1)} / (1 - \gamma_{\text{th}}^{(1)}) > 0$  for  $\gamma_{\text{th}}^{(1)} < 1$ , and then noting that  $\Pr(X < Y, X \geq Z)$  for three random variables (RVs)  $X$ ,  $Y$ , and  $Z$  can be calculated using the law of total probability as  $\Pr(X < Y, X \geq Z) = \Pr(Z \leq X < Y, Z < Y)$  since  $\Pr(Z \leq X < Y, Z \geq Y) = 0$ . Finally, step (c) follows by noting that for any constant  $C$

$$\begin{aligned}
& \mathbb{E}_{\mathcal{I}_1, \tilde{g}} \left[ \Pr\left(|\tilde{h}_2|^2 > C \left[\mathcal{I}_1 + C_{\mathcal{D}}/(a_1 L_1 P \tilde{g}^2)\right] \mid \mathcal{I}_1, \tilde{g}^2 \right) \right] \\
& \stackrel{(a)}{=} \mathbb{E}_{\mathcal{I}_1, \tilde{g}} \left[ \exp\left(-C \left[\mathcal{I}_1 + C_{\mathcal{D}}/(a_1 L_1 P \tilde{g}^2)\right]\right) \right] \\
& \stackrel{(b)}{=} \exp\left(\frac{-C \sigma_{\mathcal{R}}^2}{a_1 L_1 P}\right) \mathbb{E}_{\tilde{g}} \left[ \exp\left(\frac{-C C_{\mathcal{D}}}{a_1 L_1 P \tilde{g}^2}\right) \right] \prod_{k=1}^K \frac{a_1 L_1 P}{a_1 L_1 P + C L'_k p'_k}, \quad (8)
\end{aligned}$$

where step (a) follows from the cumulative density function (CDF) of exponential distribution  $\Pr(|\tilde{h}_2|^2 < x) = 1 - \exp(-x)$ , and (b) is obtained using the independency of  $\mathcal{I}_1$  and  $\tilde{g}$ , and then applying the independency among  $|\tilde{h}'_k|^2$ 's to get  $\mathbb{E}_{\mathcal{I}_1} [\exp(-C \mathcal{I}_1)] =$

$$\exp\left(\frac{-C \sigma_{\mathcal{R}}^2}{a_1 L_1 P}\right) \prod_{k=1}^K \mathbb{E}_{|\tilde{h}'_k|^2} \left[ \exp\left(-C L'_k p'_k |\tilde{h}'_k|^2 / (a_1 L_1 P)\right) \right].$$

Furthermore, in step (c),  $J_{\text{th},1}^{(1)} = J_{\text{th}}^{(1)} (1 + 10^{-s/10})$  and  $J_{\text{th},2}^{(1)} = \gamma_{\text{th}}^{(1)} + J_{\text{th}}^{(1)} (1 + \gamma_{\text{th}}^{(1)} \times 10^{-s/10})$ .

We should further emphasize that (7) is obtained for  $\gamma_{\text{th}}^{(1)} < 1$ . If  $\gamma_{\text{th}}^{(1)} \geq 1$ , the upper limit of  $|\tilde{h}_1|^2$  in (7) is always greater than its lower limit meaning that the condition  $(1 - \gamma_{\text{th}}^{(1)}) |\tilde{h}_2|^2 \times 10^{-s/10} < \gamma_{\text{th}}^{(1)} [\mathcal{I}_1 + C_{\mathcal{D}}/(a_1 L_1 P \tilde{g}^2)]$  holds for the all values of  $|\tilde{h}_2|^2$  and there is no need to impose such an extra condition on the calculation of the corresponding probability. As a consequence,  $\Pr(\gamma_{\pi_1}^{(1)} < \gamma_{\text{th}}^{(1)}, \pi_1)$  for  $\gamma_{\text{th}}^{(1)} \geq 1$  can be calculated as (9) shown at the top of the next page.

Finally, using (7) for  $\gamma_{\text{th}}^{(1)} < 1$  or (9) for  $\gamma_{\text{th}}^{(1)} \geq 1$ , one can obtain the coverage probability of the first NOMA user given the decoding order  $\pi_1$  as  $P_{\text{cov}|\pi_1}^{(1)} = (1 + 10^{-s/10})^{-1} - \Pr(\gamma_{\pi_1}^{(1)} < \gamma_{\text{th}}^{(1)}, \pi_1)$ . However, the closed-form characterization of  $P_{\text{cov}|\pi_1}^{(1)}$  still requires the calculation of expressions of the form  $\mathbb{E}_{\tilde{g}} [\exp(-A/\tilde{g}^2)]$ , where  $A$  is a constant and  $\tilde{g}$  is distributed according to (2). To do so, we first apply [24, Eq. (11)] and [21, Eq. (9.31.2)] to write  $\exp(-A/\tilde{g}^2)$  in the form of Meijer's G-function as  $\exp(-A/\tilde{g}^2) = G_{1,0}^{0,1} [\tilde{g}^2/A]_1^1$ . Then we can apply [24, Eq. (21)] to calculate the infinite integral of product of Meijer's G-functions involved in  $\mathbb{E}_{\tilde{g}} [\exp(-A/\tilde{g}^2)] = \int_0^\infty \exp(-A/\tilde{g}^2) f_{\tilde{g}}(\tilde{g}) d\tilde{g}$  as (10) shown at the top of the next page. For the ease of notation, hereafter, we denote  $\mathbb{E}_{\tilde{g}} [\exp(-A/\tilde{g}^2)]$  by  $\mathcal{G}(A)$  for any constant  $A$ .

Similarly, the second probability term in (6) can be obtained, first, by writing  $\Pr(\gamma_{\pi_2}^{(2)} > \gamma_{\text{th}}^{(2)}, \pi_2) = P(\pi_2) - \Pr(\gamma_{\pi_2}^{(2)} < \gamma_{\text{th}}^{(2)}, \pi_2)$ . Then using the symmetry of the problem, it can be shown that  $\Pr(\gamma_{\pi_2}^{(2)} < \gamma_{\text{th}}^{(2)}, \pi_2)$  for  $\gamma_{\text{th}}^{(2)} < 1$  and  $\gamma_{\text{th}}^{(2)} \geq 1$  can be obtained as (11) and (12), respectively, shown at the top of the next page, where  $\mathcal{G}(\cdot)$  is defined in (10), and  $J_{\text{th}}^{(2)} = 10^{-s/10} \times \gamma_{\text{th}}^{(2)} / (1 - \gamma_{\text{th}}^{(2)}) > 0$  is defined for  $\gamma_{\text{th}}^{(2)} < 1$ . Also,  $J_{\text{th},1}^{(2)} = J_{\text{th}}^{(2)} (1 + 10^{s/10})$  and  $J_{\text{th},2}^{(2)} = \gamma_{\text{th}}^{(2)} + J_{\text{th}}^{(2)} (1 + \gamma_{\text{th}}^{(2)} \times 10^{s/10})$ .

Moreover, the last probability term in (6) can be calculated by first writing

$$\begin{aligned}
\Pr(\gamma_{\pi_2}^{(1)} > \gamma_{\text{th}}^{(1)}, \pi_2) &= \Pr\left(\gamma_{\text{th}}^{(1)} \left[\mathcal{I}_1 + C_{\mathcal{D}}/(a_1 L_1 P \tilde{g}^2)\right] \right. \\
&\quad \left. < |\tilde{h}_1|^2 < |\tilde{h}_2|^2 \times 10^{-s/10}\right). \quad (14)
\end{aligned}$$

$$\Pr(\gamma_{\pi_1}^{(1)} < \gamma_{\text{th}}^{(1)}, \pi_1) \Big|_{\gamma_{\text{th}}^{(1)} \geq 1} = \frac{10^{s/10}}{1+10^{s/10}} - \frac{10^{s/10}}{\gamma_{\text{th}}^{(1)} + 10^{s/10}} \exp\left(\frac{-\gamma_{\text{th}}^{(1)} \sigma_{\mathcal{R}}^2}{a_1 L_1 P}\right) \mathbb{E}_{\tilde{g}} \left[ \exp\left(\frac{-\gamma_{\text{th}}^{(1)} C_{\mathcal{D}}}{a_1 L_1 P \tilde{g}^2}\right) \right] \prod_{k=1}^K \frac{a_1 L_1 P}{a_1 L_1 P + \gamma_{\text{th}}^{(1)} L'_k p'_k}. \quad (9)$$

$$\mathcal{G}(A) = \mathbb{E}_{\tilde{g}} [\exp(-A/\tilde{g}^2)] = \frac{\xi^2 \times 2^{\alpha+\beta-2}}{2\pi\Gamma(\alpha)\Gamma(\beta)} G_{7,2}^{0,7} \left[ \frac{16A_0^2}{A(\alpha\beta)^2} \middle| 1, (1-\xi^2)/2, (2-\xi^2)/2, (1-\alpha)/2, (2-\alpha)/2, (1-\beta)/2, (2-\beta)/2 \right]. \quad (10)$$

$$\Pr(\gamma_{\pi_2}^{(2)} < \gamma_{\text{th}}^{(2)}, \pi_2) \Big|_{\gamma_{\text{th}}^{(2)} < 1} = \frac{1}{1+10^{s/10}} \left( 1 - \exp\left(\frac{-J_{\text{th},1}^{(2)} \sigma_{\mathcal{R}}^2}{a_2 L_2 P}\right) \mathcal{G}\left(\frac{J_{\text{th},1}^{(2)} C_{\mathcal{D}}}{a_2 L_2 P}\right) \prod_{k=1}^K \frac{a_2 L_2 P}{a_2 L_2 P + J_{\text{th},1}^{(2)} L'_k p'_k} \right) - \frac{10^{-s/10}}{\gamma_{\text{th}}^{(2)} + 10^{-s/10}} \\ \times \left[ \exp\left(\frac{-\gamma_{\text{th}}^{(2)} \sigma_{\mathcal{R}}^2}{a_2 L_2 P}\right) \mathcal{G}\left(\frac{\gamma_{\text{th}}^{(2)} C_{\mathcal{D}}}{a_2 L_2 P}\right) \prod_{k=1}^K \frac{a_2 L_2 P}{a_2 L_2 P + \gamma_{\text{th}}^{(2)} L'_k p'_k} - \exp\left(\frac{-\sigma_{\mathcal{R}}^2 J_{\text{th},2}^{(2)}}{a_2 L_2 P}\right) \mathcal{G}\left(\frac{C_{\mathcal{D}} J_{\text{th},2}^{(2)}}{a_2 L_2 P}\right) \prod_{k=1}^K \frac{a_2 L_2 P}{a_2 L_2 P + L'_k p'_k J_{\text{th},2}^{(2)}} \right]. \quad (11)$$

$$\Pr(\gamma_{\pi_2}^{(2)} < \gamma_{\text{th}}^{(2)}, \pi_2) \Big|_{\gamma_{\text{th}}^{(2)} \geq 1} = \frac{1}{1+10^{s/10}} - \frac{10^{-s/10}}{\gamma_{\text{th}}^{(2)} + 10^{-s/10}} \exp\left(\frac{-\gamma_{\text{th}}^{(2)} \sigma_{\mathcal{R}}^2}{a_2 L_2 P}\right) \mathcal{G}\left(\frac{\gamma_{\text{th}}^{(2)} C_{\mathcal{D}}}{a_2 L_2 P}\right) \prod_{k=1}^K \frac{a_2 L_2 P}{a_2 L_2 P + \gamma_{\text{th}}^{(2)} L'_k p'_k}. \quad (12)$$

$$\Pr(\gamma_{\pi_2}^{(1)} > \gamma_{\text{th}}^{(1)}, \pi_2) = \frac{1}{1+10^{s/10}} \times \exp\left(\frac{-\gamma_{\text{th}}^{(1)} \sigma_{\mathcal{R}}^2 (1+10^{s/10})}{a_1 L_1 P}\right) \mathcal{G}\left(\frac{\gamma_{\text{th}}^{(1)} C_{\mathcal{D}} (1+10^{s/10})}{a_1 L_1 P}\right) \prod_{k=1}^K \frac{a_1 L_1 P}{a_1 L_1 P + \gamma_{\text{th}}^{(1)} L'_k p'_k (1+10^{s/10})}. \quad (13)$$

Then using a similar approach to (7), the closed-form expression for all values of  $\gamma_{\text{th}}^{(1)}$  can be expressed as (13) shown at the top of this page. This completes the closed-form characterization of the outage probability of the first NOMA user  $\mathcal{U}_1$ .

Finally, the outage probability of the second NOMA user  $\mathcal{U}_2$  can be characterized as

$$P_{\text{out}}^{(2)} = 1 - \left[ \Pr(\gamma_{\pi_2}^{(2)} > \gamma_{\text{th}}^{(2)}, \pi_2) + \Pr(\gamma_{\pi_1}^{(1)} > \gamma_{\text{th}}^{(1)}, \pi_1) \times \Pr(\gamma_{\pi_1}^{(2)} > \gamma_{\text{th}}^{(2)}, \pi_1) / P(\pi_1) \right], \quad (15)$$

where  $\Pr(\gamma_{\pi_2}^{(2)} > \gamma_{\text{th}}^{(2)}, \pi_2)$  and  $\Pr(\gamma_{\pi_1}^{(1)} > \gamma_{\text{th}}^{(1)}, \pi_1)$  have already been calculated, and  $\Pr(\gamma_{\pi_1}^{(2)} > \gamma_{\text{th}}^{(2)}, \pi_1)$  can be obtained as

$$\Pr(\gamma_{\pi_1}^{(2)} > \gamma_{\text{th}}^{(2)}, \pi_1) = (1 + 10^{-s/10})^{-1} \times \exp\left(\frac{-\gamma_{\text{th}}^{(2)} \sigma_{\mathcal{R}}^2 (1+10^{-s/10})}{a_2 L_2 P}\right) \mathcal{G}\left(\frac{\gamma_{\text{th}}^{(2)} C_{\mathcal{D}} (1+10^{-s/10})}{a_2 L_2 P}\right) \\ \times \prod_{k=1}^K \frac{a_2 L_2 P}{a_2 L_2 P + \gamma_{\text{th}}^{(2)} L'_k p'_k (1+10^{-s/10})}. \quad (16)$$

This means that the outage probability of the second NOMA user can be characterized using the preceding analysis by substituting  $-s$  for  $s$  and appropriate change of indexing  $1 \leftrightarrow 2$ . This is because the only difference between  $\mathcal{U}_1$  and  $\mathcal{U}_2$  is that the user with a lower average gain is labeled as the second user, i.e.,  $a_2 L_2 = a_1 L_1 \times 10^{-s/10}$ .

### B. Sum-Rate Outage Analysis

Assuming that the data rate of the  $i$ -th NOMA user for the  $j$ -th decoding order is related to the corresponding SINR as  $R_{\pi_j}^{(i)} = \log_2(1 + \gamma_{\pi_j}^{(i)})$ ,  $i, j \in \{1, 2\}$ , then it is easy to verify that the sum rate of the NOMA users, regardless of their decoding order, can be expressed as

$$R_{\Sigma} = \log_2 \left( 1 + \frac{a_1 L_1 P \tilde{g}^2 |\tilde{h}_1|^2 + a_2 L_2 P \tilde{g}^2 |\tilde{h}_2|^2}{\sum_{k=1}^K L'_k p'_k \tilde{g}^2 |\tilde{h}_k|^2 + \tilde{g}^2 \sigma_{\mathcal{R}}^2 + C_{\mathcal{D}}} \right). \quad (17)$$

Denoting the fractional term of the logarithm argument in (17) by  $\gamma_{\Sigma}$ , the sum-rate outage probability defined as  $P_{\text{out}}^{\Sigma} = \Pr(\gamma_{\Sigma} < \gamma_{\text{th}}^{\Sigma})$ , where  $\gamma_{\text{th}}^{\Sigma} = 2^{R_{\text{th}}^{\Sigma}} - 1$  is the threshold equivalent SINR to achieve the desired sum-rate of  $R_{\text{th}}^{\Sigma}$ , can be expressed as

$$P_{\text{out}}^{\Sigma} = \Pr \left( |\tilde{h}_1|^2 < \gamma_{\text{th}}^{\Sigma} [\mathcal{I}_1 + C_{\mathcal{D}} / (a_1 L_1 P \tilde{g}^2)] - |\tilde{h}_2|^2 \times 10^{-s/10} \right). \quad (18)$$

Let  $\mathcal{B}$  represent the event  $\{|\tilde{h}_2|^2 < \gamma_{\text{th}}^{\Sigma} \times 10^{s/10} [\mathcal{I}_1 + C_{\mathcal{D}} / (a_1 L_1 P \tilde{g}^2)]\}$ , and

$$\mathcal{SO} = \{|\tilde{h}_1|^2 < \gamma_{\text{th}}^{\Sigma} [\mathcal{I}_1 + C_{\mathcal{D}} / (a_1 L_1 P \tilde{g}^2)] - |\tilde{h}_2|^2 \times 10^{-s/10}\}, \quad (19)$$

i.e., the sum-rate outage event defined in (18). Clearly,  $\Pr(\mathcal{SO}, \mathcal{B}^c) = 0$  where  $\mathcal{B}^c$  is the complementary event of  $\mathcal{B}$ . Therefore, using the law of total probability,  $P_{\text{out}}^{\Sigma}$  can be expressed as  $P_{\text{out}}^{\Sigma} = \Pr(\mathcal{SO}, \mathcal{B})$  which is calculated in a closed-form as (20) at the top of the next page.

It is worth remarking at this point that in the special case of absence of multiuser interference (except the NOMA users themselves), one can obtain the outage probability closed-form expressions by substituting  $L'_k p'_k = 0$ ,  $\forall k = 1, 2, \dots, K$ , which replaces all the product terms of the form  $\prod_{k=1}^K [\cdot]$  by 1.

## IV. NUMERICAL RESULTS

In this section, we present the numerical results to evaluate the performance of uplink NOMA over mixed RF-FSO systems, and corroborate the correctness of the derived outage probability closed forms. Some of the parameters considered for simulations are listed in Table I. For the multiuser interference, we consider the product of  $L'_k p'_k$ ,  $k = 1, 2, \dots, K$ , to be the  $k$ -th element of the vector  $K_{\mathcal{I}} P_0 L_2 \mathbf{u}_{10}$  where  $P_0 = 1$  mW,  $K_{\mathcal{I}} \geq 0$  is a constant to define the upper bound of the received power from each interfering user as a factor of  $P_0 L_2$ , and  $\mathbf{u}_{10} = (0.6957, 0.6279, 0.4504, 0.4736, 0.9497, 0.0835, 0.2798, 0.4470, 0.5876, 0.8776)$  is a length-10 vector of uniformly generated numbers over the interval  $(0, 1)$ .

$$\begin{aligned}
P_{\text{out}}^{\Sigma} &= \mathbb{E}_{|\tilde{h}_2|^2 < \gamma_{\text{th}}^{\Sigma} \times 10^{s/10}} \left[ \mathbf{z}_1 + C_{\mathcal{D}} / (a_1 L_1 P \tilde{g}^2) \right] \left[ 1 - \exp \left( -\gamma_{\text{th}}^{\Sigma} \left[ \mathbf{z}_1 + C_{\mathcal{D}} / (a_1 L_1 P \tilde{g}^2) \right] + |\tilde{h}_2|^2 \times 10^{-s/10} \right) \right] \\
&= 1 + \frac{1}{10^{s/10} - 1} \times \exp \left( \frac{-\sigma_{\mathcal{R}}^2 \gamma_{\text{th}}^{\Sigma} \times 10^{s/10}}{a_1 L_1 P} \right) \mathcal{G} \left( \frac{C_{\mathcal{D}} \gamma_{\text{th}}^{\Sigma} \times 10^{s/10}}{a_1 L_1 P} \right) \prod_{k=1}^K \frac{a_1 L_1 P}{a_1 L_1 P + L'_k p'_k \gamma_{\text{th}}^{\Sigma} \times 10^{s/10}} \\
&\quad - \frac{10^{s/10}}{10^{s/10} - 1} \times \exp \left( \frac{-\gamma_{\text{th}}^{\Sigma} \sigma_{\mathcal{R}}^2}{a_1 L_1 P} \right) \mathcal{G} \left( \frac{\gamma_{\text{th}}^{\Sigma} C_{\mathcal{D}}}{a_1 L_1 P} \right) \prod_{k=1}^K \frac{a_1 L_1 P}{a_1 L_1 P + \gamma_{\text{th}}^{\Sigma} L'_k p'_k}.
\end{aligned} \tag{20}$$

Table I  
SOME OF THE IMPORTANT PARAMETERS USED FOR SIMULATIONS.

Coefficient	Value
Responsivity of the photodetector, $\rho$	$0.5 \text{ V}^{-1}$
Electrical-to-optical conversion coefficient, $\eta$	1
Receiver aperture radius, $r$	10 cm
Transmitter beam divergence angle, $\phi$	2 mrad
Noise power at the relay RF receiver, $\sigma_{\mathcal{R}}^2$	-80 dBm
Noise variance at the destination FSO receiver, $\sigma_{\mathcal{D}}^2$	$10^{-14} \text{ A}^2$
Number of interfering users to relay, $K$	10
Number of iterations for numerical simulations, $N_t$	$10^6$
Gamma-Gamma turbulence parameters, $(\alpha, \beta)$	(10, 5)
Length of the FSO backhaul link, $d_{\mathcal{R}\mathcal{D}}$	800 m
Weather-dependent attenuation coefficient, $\kappa$	$0.02 \text{ m}^{-1}$

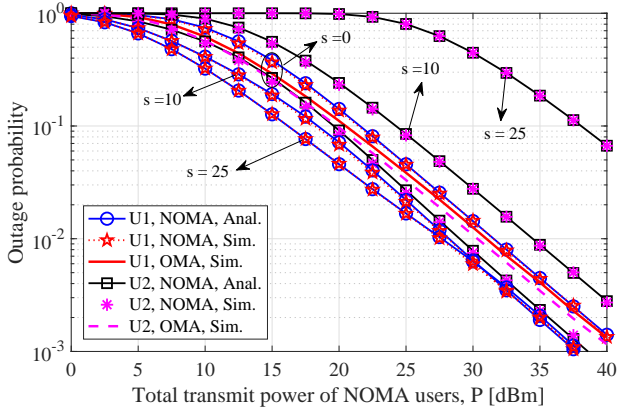


Figure 1. Individual-rate outage probability results of the mixed RF-FSO NOMA system for three values of power back-off step  $s = 0, 10,$  and  $25$  dB. The other specific parameters are  $\gamma_{\text{th}}^{(1)} = 0.8, \gamma_{\text{th}}^{(2)} = 0.4, L_1 = 2 \times 10^{-7}, L_2 = 10^{-7}, K_{\mathcal{I}} = 1, \zeta = 2,$  and  $G = 100$ .

Figure 1 shows the individual-rate outage performance of the uplink mixed RF-FSO NOMA system for three different values of the power back-off step. For  $s = 0$  we will have  $a_1 L_1 = a_2 L_2$ ; therefore, one should expect a lower outage probability for the second NOMA user given its lower threshold SINR. However, by increasing  $s$  a larger fraction of power will be assigned to the first NOMA user, and  $\mathcal{U}_1$  achieves lower outage probabilities even if it has a larger SINR threshold. As a consequence, increasing  $s$  will decrease the outage probability of  $\mathcal{U}_1$  and increase the outage probability of  $\mathcal{U}_2$ . Moreover, the excellent match between the analytical results and Monte-Carlo numerical simulations corroborate the correctness of the derived closed-form expressions for the individual-rate outage probabilities.

The comparison between NOMA and OMA is also depicted in Figure 1. To do so, we assume, for OMA operation, that the total transmission time is equally divided between the two users and each user employs the entire transmission power  $P$

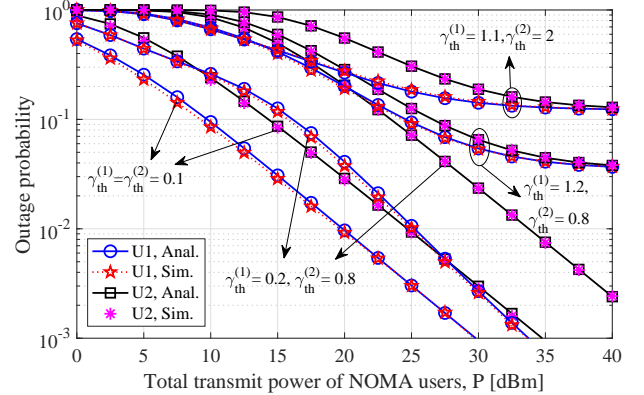


Figure 2. Individual-rate outage probability results of the mixed RF-FSO NOMA system for power back-off step  $s = 5$  dB, and different values of threshold SINRs. The other parameters are the same as Figure 1.

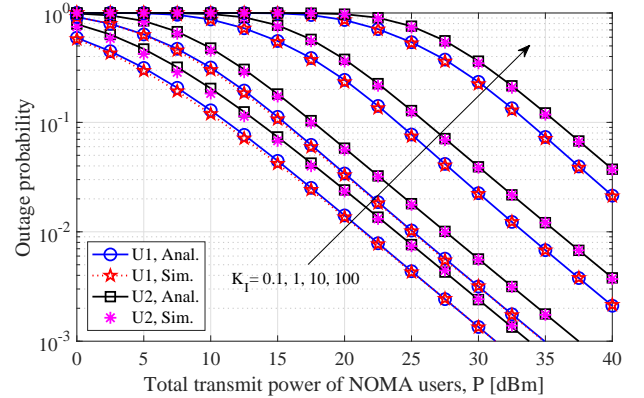


Figure 3. Individual-rate outage probability results of the mixed RF-FSO NOMA system for power back-off step  $s = 5$  dB,  $\gamma_{\text{th}}^{(1)} = 0.7, \gamma_{\text{th}}^{(2)} = 0.4, L_1 = 10^{-6}, L_2 = 2 \times 10^{-7}, \zeta = 2, G = 100,$  and different values of  $K_{\mathcal{I}}$ .

during its corresponding time slot. Then it is easy to verify that, in order to achieve the target data rate  $R_{\text{th}}^{(i)} = \log_2(1 + \gamma_{\text{th}}^{(i)})$ ,  $i \in \{1, 2\}$ , each  $i$ -th OMA user has to satisfy the threshold SNR of  $\gamma_{\text{th}, \text{OMA}}^{(i)} = (1 + \gamma_{\text{th}}^{(i)})^2 - 1$ . It is observed that NOMA operation is in favor of the first user except for very small values of  $s$  while the second user experiences an opposite situation.

Figure 2 illustrates the individual-rate outage performance of the system for  $s = 5$  dB and different values of threshold SINRs. As expected, outage performance degrades with increasing the threshold SINRs. More importantly, the induced interference between NOMA users due to the non-orthogonal operation limits the outage performance for large values of threshold SINRs and prevents achieving small enough outage probabilities even for large values of the transmitted power. Consequently, the system performance saturates where the saturation limit is larger for the larger values of threshold SINRs.

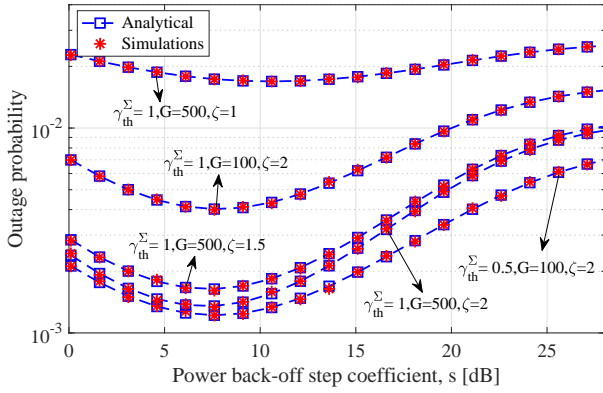


Figure 4. Sum-rate outage probability results of the mixed RF-FSO NOMA system for  $L_1 = 10^{-6}$ ,  $L_2 = 2 \times 10^{-7}$ ,  $P = 20$  dBm,  $K_{\mathcal{I}} = 1$ , and different values of  $\gamma_{\text{th}}^{\Sigma}$ ,  $\zeta$ , and  $G$ .

The impact of multiuser interference on the individual-rate outage performance of NOMA users is investigated in Figure 3 where a significant performance degradation is observed for relatively strong interference regimes. Note that even for  $K_{\mathcal{I}} = 1$  which is equivalent to having interfering users with the same path loss gain of  $L_2$  as the second NOMA user and transmit powers bounded by  $P_0 = 0$  dBm, one can observe about 4 dB of performance degradation compared to  $K_{\mathcal{I}} = 0.1$  at the outage probability  $10^{-3}$ .

The sum-rate outage performance of the system is characterized in Figure 4 for  $P = 20$  dBm and different values of  $\gamma_{\text{th}}^{\Sigma}$ ,  $\zeta$ , and  $G$ . As expected, the outage performance increases for larger values of the threshold SINR  $\gamma_{\text{th}}^{\Sigma}$ , smaller values of the relay gain  $G$ , and higher pointing errors (equivalently, smaller  $\zeta$ ). Furthermore, given any set of system parameters, there is unique power back-off step  $s^*$  minimizing the sum-rate outage probability. However, such a  $s^*$  is not necessarily the best operation point as such an operation region may depend to the individual outage probabilities and achievable rates and not only to the sum-rate outage probability. More importantly, it is observed that the performance degradation due to the laser beam misalignment can be quite remarkable. This necessitates hybrid design of the backhaul link to incorporate an RF or millimeter wave link as a backup to assist the FSO backhaul link in the case of poor transmission quality of the FSO link. Such designs are necessary to guarantee the users requirements for high reliability and low latency, and will be explored in our future work.

## V. CONCLUSIONS

In this paper, we derived the closed-form expressions for the individual- and sum-rate outage probabilities of dual-hop uplink NOMA over mixed RF-FSO systems with Rayleigh fading for the users-relay access links, multiuser interference to the relay, Gamma-Gamma turbulence with pointing error for the FSO backhaul link, and dynamic-order decoding at the destination. This work can be regarded as an initial attempt to incorporate ultra-high-throughput FSO links as an effective backhauling solution to meet the ever-increasing demand of users for higher data rates and the stringent requirements of reliability and latency for variety of emerging applications. The analysis in this paper are performed for general cases and their validity is verified through extensive numerical results.

## REFERENCES

- [1] L. Dai, B. Wang, Y. Yuan, S. Han, I. Chih-Lin, and Z. Wang, "Non-orthogonal multiple access for 5G: Solutions, challenges, opportunities, and future research trends," *IEEE Commun. Mag.*, vol. 53, no. 9, pp. 74–81, 2015.
- [2] Z. Ding, X. Lei, G. K. Karagiannidis, R. Schober, J. Yuan, and V. K. Bhargava, "A survey on non-orthogonal multiple access for 5G networks: Research challenges and future trends," *IEEE J. Sel. Areas Commun.*, vol. 35, no. 10, pp. 2181–2195, 2017.
- [3] J.-B. Kim and I.-H. Lee, "Capacity analysis of cooperative relaying systems using non-orthogonal multiple access," *IEEE Commun. Lett.*, vol. 19, no. 11, pp. 1949–1952, 2015.
- [4] C. Zhong and Z. Zhang, "Non-orthogonal multiple access with cooperative full-duplex relaying," *IEEE Commun. Lett.*, vol. 20, no. 12, pp. 2478–2481, 2016.
- [5] J. Men and J. Ge, "Non-orthogonal multiple access for multiple-antenna relaying networks," *IEEE Commun. Lett.*, vol. 19, no. 10, pp. 1686–1689, 2015.
- [6] J. Men, J. Ge, and C. Zhang, "Performance analysis of nonorthogonal multiple access for relaying networks over Nakagami- $m$  fading channels," *IEEE Trans. Veh. Technol.*, vol. 66, no. 2, pp. 1200–1208, 2017.
- [7] J.-B. Kim and I.-H. Lee, "Non-orthogonal multiple access in coordinated direct and relay transmission," *IEEE Commun. Lett.*, vol. 19, no. 11, pp. 2037–2040, 2015.
- [8] M. F. Kader and S. Y. Shin, "Coordinated direct and relay transmission using uplink NOMA," *IEEE Wireless Commun. Lett.*, vol. 7, no. 3, pp. 400–403, 2018.
- [9] Y. Liu, G. Pan, H. Zhang, and M. Song, "Hybrid decode-forward & amplify-forward relaying with non-orthogonal multiple access," *IEEE Access*, vol. 4, pp. 4912–4921, 2016.
- [10] Y. Xiao, L. Hao, Z. Ma, Z. Ding, Z. Zhang, and P. Fan, "Forwarding strategy selection in dual-hop NOMA relaying systems," *IEEE Commun. Lett.*, to appear, Feb. 2018.
- [11] M. V. Jamali and H. MahdaviFar, "A low-complexity recursive approach toward code-domain NOMA for massive communications," *arXiv preprint arXiv:1804.05242*, 2018.
- [12] X. Ge, H. Cheng, M. Guizani, and T. Han, "5G wireless backhaul networks: challenges and research advances," *IEEE Network*, vol. 28, no. 6, pp. 6–11, 2014.
- [13] F. Demers, H. Yanikomeroglu, and M. St-Hilaire, "A survey of opportunities for free space optics in next generation cellular networks," in *Communication Networks and Services Research Conference (CNSR), 2011 Ninth Annual*. IEEE, 2011, pp. 210–216.
- [14] J. G. Andrews, T. Bai, M. N. Kulkarni, A. Alkhatieb, A. K. Gupta, and R. W. Heath, "Modeling and analyzing millimeter wave cellular systems," *IEEE Trans. Commun.*, vol. 65, no. 1, pp. 403–430, 2017.
- [15] M. A. Khalighi and M. Uysal, "Survey on free space optical communication: A communication theory perspective," *IEEE Commun. Surveys Tuts*, vol. 16, no. 4, pp. 2231–2258, 2014.
- [16] Y. Gao, B. Xia, K. Xiao, Z. Chen, X. Li, and S. Zhang, "Theoretical analysis of the dynamic decode ordering SIC receiver for uplink NOMA systems," *IEEE Commun. Lett.*, vol. 21, no. 10, pp. 2246–2249, 2017.
- [17] M. Najafi, V. Jamali, P. D. Diamantoulakis, G. K. Karagiannidis, and R. Schober, "Non-orthogonal multiple access for FSO backhauling," in *Wireless Communications and Networking Conference (WCNC), 2018 IEEE*. IEEE, 2018, pp. 1–6.
- [18] V. Jamali, D. S. Michalopoulos, M. Uysal, and R. Schober, "Link allocation for multiuser systems with hybrid RF/FSO backhaul: Delay-limited and delay-tolerant designs," *IEEE Trans. Wireless Commun.*, vol. 15, no. 5, pp. 3281–3295, 2016.
- [19] E. Lee, J. Park, D. Han, and G. Yoon, "Performance analysis of the asymmetric dual-hop relay transmission with mixed RF/FSO links," *IEEE Photonics Technol. Lett.*, vol. 23, no. 21, pp. 1642–1644, 2011.
- [20] H. G. Sandalidis, T. A. Tsiftsis, and G. K. Karagiannidis, "Optical wireless communications with heterodyne detection over turbulence channels with pointing errors," *J. Lightw. Technol.*, vol. 27, no. 20, pp. 4440–4445, 2009.
- [21] I. S. Gradshteyn and I. M. Ryzhik, *Table of integrals, series, and products*. Academic Press, 2007.
- [22] N. Zhang, J. Wang, G. Kang, and Y. Liu, "Uplink nonorthogonal multiple access in 5G systems," *IEEE Commun. Lett.*, vol. 20, no. 3, pp. 458–461, 2016.
- [23] Z. Yang, Z. Ding, P. Fan, and N. Al-Dhahir, "A general power allocation scheme to guarantee quality of service in downlink and uplink NOMA systems," *IEEE Trans. Wireless Commun.*, vol. 15, no. 11, pp. 7244–7257, 2016.
- [24] V. Adamchik and O. Marichev, "The algorithm for calculating integrals of hypergeometric type functions and its realization in reduce system," in *Proc. Int. Conf. Symbolic and Algebraic Computation*. ACM, Tokyo, Japan, 1990, pp. 212–224.